Journal of Solid State Chemistry 278 (2019) 120921

Contents lists available at ScienceDirect

Journal of Solid State Chemistry

journal homepage: www.elsevier.com/locate/jssc

High-pressure synthesis of A-site ordered perovskite $CaMn_3(Fe_3Mn)O_{12}$ and sequential long-range antiferromagnetic ordering and spin glass transition

Jia Guo [a,b], Xubin Ye [a,b], Zhehong Liu [a,b], Weipeng Wang [a,b], Shijun Qin [a,b], Bowen Zhou [a,b], Zhiwei Hu [c], Hong-Ji Lin [d], Chien-Te Chen [d], Richeng Yu [a,b], Liu Hao Tjeng [c], Youwen Long [a,b,e,*]

[a] Beijing National Laboratory for Condensed Matter Physics, Institute of Physics, Chinese Academy of Sciences, Beijing, 100190, China
[b] School of Physical Sciences, University of Chinese Academy of Sciences, Beijing, 100049, China
[c] Max Planck Institute for Chemical Physics of Solids, Dresden, 01187, Germany
[d] National Synchrotron Radiation Research Center, Hsinchu, 30076, Taiwan, ROC
[e] Songshan Lake Materials Laboratory, Dongguan, Guangdong, 523808, China

ARTICLE INFO

Keywords:
High pressure synthesis
A-site ordered perovskite
Spin ordering
Spin glass

ABSTRACT

An $AA'_3B_4O_{12}$-type perovskite oxide $CaMn_3(Fe_3Mn)O_{12}$ was synthesized at 8 GPa and 1473 K. X-ray diffraction shows a cubic crystal structure with space group *Im*-3. The charge states are verified by soft x-ray absorption spectroscopy to be $CaMn^{3+}{}_3(Fe^{3+}{}_3Mn^{4+})O_{12}$, where the Ca^{2+} and Mn^{3+} are 1:3 ordered respectively at A and A′ sites, while the Mn^{4+} and Fe^{3+} are disorderly distributed at B site. The spin interaction of A′-site Mn^{3+} ions causes a long-range antiferromagnetic phase transition at about 39 K. Subsequently, a spin glass transition is found to occur around 14 K due to the randomly distributed Fe^{3+} and Mn^{4+} at B site. Moreover, the spin glass behavior follows a dynamic scaling power law. The temperature dependent resistivity can be well fitted by a 3D Mott variable-range hopping model, indicating the insulating nature of $CaMn_3(Fe_3Mn)O_{12}$ due to the strong electron correlation effects.

1. Introduction

A-site ordered perovskite oxides with chemical formula $AA'_3B_4O_{12}$ attract considerable attention due to the special crystal structure and interesting physical properties, such as intermetallic charge transfer [1–5], half metallicity [6,7], charge disproportionation [8–10], colossal magnetoresistance [6,11–13], giant dielectric constant [14,15], magnetoelectric multiferroicity [16,17], and negative thermal expansion [1,18], etc. In this structure (see Fig. 1a), both A′ and B sites can accommodate transition metals, forming $A'O_4$ square and BO_6 octahedral coordination units, respectively. Correspondingly, a transition-metal cation with first-order Jahn–Teller effect like Cu^{2+} ($t_{2g}^6e_g^3$) or Mn^{3+} ($t_{2g}^3e_g^1$) is favorable to occupy the A′ site [19]. In most $ACu_3B_4O_{12}$ compounds, there exist strong spin interactions between A′-site Cu and B-site transition metals, giving rise to a single magnetic phase transition with a higher ordering temperature [20,21]. For example, $CaCu_3Mn_4O_{12}$ and $BiCu_3Mn_4O_{12}$ experience a Cu(↑)Mn(↓) ferrimagnetic phase transition near 350 K [13,22]. In contrast to the single magnetic transition, two antiferromagnetic (AFM) phase transitions are usually found to occur in $AMn_3B_4O_{12}$. One originates from the B-site magnetic ions, and the other from the A′-site Mn^{3+} spins [16,17,23]. As an instance, in $LaMn_3Cr_4O_{12}$ the B-site Cr^{3+} ions cause a long-rang AFM transition at 150 K, while the A′-site Mn^{3+} ions lead to another one around 50 K [24]. Moreover, the total spin structure composed of Cr^{3+} and Mn^{3+} can break special inversion symmetry and therefore induce ferroelectric polarization [16,25].

$CaMn_7O_{12}$ ($CaMn_3Mn_4O_{12}$) is a peculiar system, in which both A′ and B sites are occupied by the same 3d transition metal Mn. Above 440 K, $CaMn^{3+}{}_3Mn^{3.25+}{}_4O_{12}$ possesses an A-site order perovskite structure with a cubic *Im*-3 symmetry containing a mixed $Mn^{3.25+}$ valence state at the B site [26–28]. Below this temperature, however, the crystal structure changes to both A- and B-site ordered perovskite $CaMn^{3+}{}_3(Mn^{3+}{}_3Mn^{4+})O_{12}$ with space group of *R*-3 [29]. In addition, special orbital ordering is claimed to occur at lower temperatures [30,31]. More interestingly, $CaMn_7O_{12}$ is a magnetoelectric multiferroic material with a high ferroelectric critical temperature and large polarization [23,26,32]. Neutron diffraction reveals complex spin interactions in $CaMn_7O_{12}$ [28,33], where the structure and magnetism are sensitive to B-site substitution [34]. Since Fe^{3+} has similar ionic radius with that of Mn^{3+} [35] but much more d-electrons, in this paper, we apply high-pressure synthesis

* Corresponding author. Beijing National Laboratory for Condensed Matter Physics, Institute of Physics, Chinese Academy of Sciences, Beijing, 100190, China.
E-mail address: ywlong@iphy.ac.cn (Y. Long).

https://doi.org/10.1016/j.jssc.2019.120921
Received 15 July 2019; Received in revised form 18 August 2019; Accepted 21 August 2019
Available online 22 August 2019

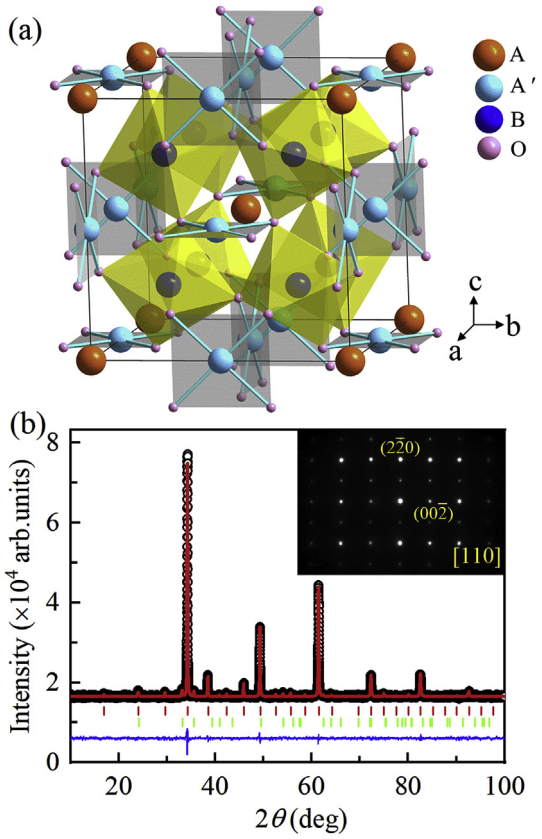

Fig. 1. (a) Crystal structure of A-site ordered quadruple perovskite with *Im*-3 symmetry. (b) XRD pattern collected at room temperature and Rietveld refinement results for $CaMn_3Fe_3MnO_{12}$. Observed (circles), calculated (red line), and difference (bottom line) profiles are shown. The red ticks indicate the allowed Bragg reflections with space group *Im*-3. The green ticks indicate the Bragg reflections arising from a small amount of α-Fe_2O_3 impurity phase (~5 wt%). (For interpretation of the references to colour in this figure legend, the reader is referred to the Web version of this article.)

conditions to substitute all the B-site Mn^{3+} in $CaMn^{3+}{}_3(Mn^{3+}{}_3Mn^{4+})O_{12}$ and prepare $CaMn_3Fe_3MnO_{12}$ (CMFMO). The crystal structure, magnetic, electrical, and specific heat properties are reported.

2. Experimental

Polycrystalline CMFMO was synthesized under 8 GPa and 1473 K for 30 min by using a cubic-anvil-type high-pressure apparatus. Highly pure (>99.9%) $CaMnO_3$, Fe_2O_3, Fe and MnO_2 powders were used as starting materials. The $CaMnO_3$ was synthesized from a mixture of $CaCO_3$ and MnO_2 as reported elsewhere [36]. The powders with a 1:1:1:3 mol ratio were fully mixed in an agate mortar within a glovebox filled with Ar gas. The mixed powders were sealed into a Pt capsule with 3.0 mm in diameter and 4.0 mm in length for high pressure treatment. Powder X-ray diffraction (XRD) was performed using a Huber diffractometer equipped with Cu–Kα1 radiation at 40 kV and 30 mA. The sample was scanned in the angle range from 10° to 100° with a 0.005° resolution. The XRD data were analyzed by the Rietveld full-profile refinement [37] with the GSAS program [38]. A Philips-CM200 field emission transmission electron microscope was used to perform high-resolution selected area electron diffraction (SAED) at room temperature along the [110] zone. The valence states of Mn and Fe of CMFMO, together with $YMn_3Al_4O_{12}$ and $LaFeO_3$ as references were studied by soft X-ray absorption spectroscopy (XAS) at the Mn-$L_{2,3}$ edges and the Fe-$L_{2,3}$ edges at the 11A beamline of the National Synchrotron Radiation Research Center in Taiwan using the total electron yield mode. A single crystal MnO and a single crystal Fe_2O_3 were simultaneously measured for energy references at the Mn-$L_{2,3}$ and the Fe-$L_{2,3}$ edges, respectively. A superconducting quantum interference device magnetometer (MPMS3, Quantum Design) was used to measure the magnetic susceptibility and magnetization. The zero-field-cooling (ZFC) and field-cooling (FC) susceptibility data were collected under 0.05 and 0.5 T. The magnetization curves were measured from -7 to +7 T at several temperatures of 200, 50, 30 and 2 K. A physical property measurement system (Quantum Design, PPMS-9T) was used to measure the temperature dependence of the ac magnetization (M'), resistivity and specific heat.

3. Results and discussion

Fig. 1b shows the XRD pattern measured at room temperature and the related refinement results for CMFMO. The Rietveld analysis shows that CMFMO has an A-site ordered quadruple perovskite structure with space group *Im*-3. This means that A-site Ca and A′-site Mn are distributed orderly with a ratio of 1:3, whereas the B-site Mn and Fe are arranged randomly. To further confirm the B-site disorder, the SAED was performed along the [110] zone axis. As shown in the inset of Fig. 1b, one cannot distinguish any diffraction spots with $h + k + l =$ odd, revealing the disorder distribution for B-site Mn and Fe [39,40]. In *Im*-3 symmetry, the A-site Ca atoms and A′-site Mn atoms occupy the 2*a* (0, 0, 0) and 6*b* (0, 0.5, 0.5) positions, respectively; the B-site Mn/Fe atoms are located at the special site 8*c* (0.25, 0.25, 0.25), and O atoms at 24*g* (0, *y*, *z*). Table 1 lists the refined structure parameters such as lattice constant, atomic positions, bond length and angle etc. According to the A′-site Mn–O bond length, the bond valence sum (BVS) [41,42] calculations show that the valence state of Mn at this site is +2.75, suggesting the presence of a Mn^{3+} state.

The XAS technique is applied to verify the valence states of Mn and Fe. Fig. 2a shows the Mn-$L_{2,3}$ XAS spectra of CMFMO, and of $YMn^{3+}{}_3Al_4O_{12}$ (YMAO) as a Mn^{3+} reference with MnO_4 square coordination [43], and La_2MnCoO_6 (LMCO) taken from Ref. [44], as a Mn^{4+} reference with MnO_6 octahedral coordination. One can see that the absorption spectrum of CMFMO displays mixed features from those of YMAO and LMCO. It means that both square-coordinated Mn^{3+} and octahedral-coordinated Mn^{4+} are involved in CMFMO. Actually, a simple XAS superposition of YMAO and LMCO with a 3:1 ratio (see the magenta line in Fig. 2a) can well reproduce the spectrum of CMFMO, confirming the formation of Mn^{3+} state at the A site and Mn^{4+} state at the B site. Fig. 2b shows the Fe-$L_{2,3}$ XAS spectrum of CMFMO together with that of $LaFeO_3$ with a similar FeO_6 octahedral coordination. Obviously, these two compounds have similar energy position and spectral shape demonstrating the presence of Fe^{3+} state with octahedral coordination in CMFMO. The XAS results thus confirm the charge combination of

Table 1
Refined structure parameters of $CaMn_3Fe_3MnO_{12}$ at room temperature. Space group: *Im*-3; Atomic sites: Ca 2*a* (0, 0, 0), Mn 6*b* (0, 0.5, 0.5), Mn/Fe 8*c* (0.25, 0.25, 0.25), O 24*g* (0, *y*, *z*).

Parameter	CMFMO
a(Å)	7.38086(1)
O_y	0.1779(4)
O_z	0.3113(4)
U_{iso} (Ca) (100 × Å^2)	0.24(8)
U_{iso} (Mn) (100 × Å^2)	1.12(2)
U_{iso} (Fe) (100 × Å^2)	0.46(1)
U_{iso} (O) (100 × Å^2)	0.42(5)
Mn–O (× 4 Å)	1.914(3)
(× 4 Å)	2.756(3)
(× 4 Å)	3.307(3)
∠Mn–O–Mn (deg)	102.9(1)
∠Fe–O–Fe (deg)	138.5(1)
R_{wp} (%)	1.37
R_p (%)	1.02

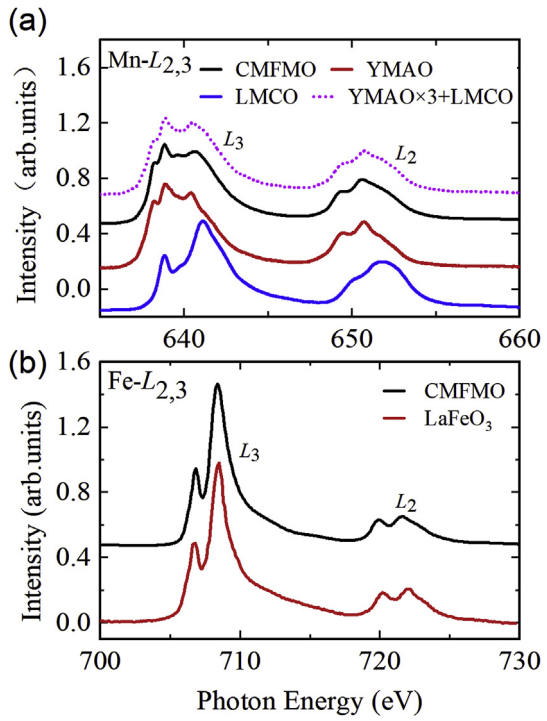

Fig. 2. (a) The Mn-$L_{2,3}$ XAS spectra of CMFMO (black) and the references $YMn^{3+}{}_3Al_4O_{12}$ and $La_2Mn^{4+}CoO_6$ (LMCO blue from Ref. [44]). The magenta dot line stands for a simple superposition of YMAO and LMCO with a 3:1 ratio. (b) The Fe-$L_{2,3}$ XAS spectra of CMFMO (black) and the reference $LaFe^{3+}O_3$ (red). (For interpretation of the references to colour in this figure legend, the reader is referred to the Web version of this article.)

$CaMn^{3+}{}_3(Fe^{3+}{}_3Mn^{4+})O_{12}$ in agreement with the BVS calculations.

Considering that both A′- and B-site atoms are accommodated by magnetic transition-metal ions, it is interesting to study the magnetism of CMFMO. Fig. 3a shows the ZFC and FC susceptibility curves measured at 0.05 and 0.5 T. The susceptibility shows similar features at these two fields. With decreasing temperature, the ZFC curve experiences a sharp anomaly at $T_N \approx 39$ K, followed by another broadening one around $T_{SG} \approx 14$ K. As will be shown by ac magnetization later, the magnetic transition occurring at T_N is independent on measurement frequency, while the lower-temperature one changes considerably. Therefore, a long-range AFM ordering is assigned at the onset of 39 K, whereas a spin glass transition takes place near 14 K in the current CMFMO. As shown in Fig. 3a, the ZFC and FC susceptibility curves separate for each other below T_N. It may imply a canted AFM ordering and/or the formation of some short-range spin interactions. Fig. 3b shows the inverse susceptibility as a function of temperature. Between 200 and 300 K, the data can be well fitted based on the modified Curie-Weiss law with the function $\chi = \chi_0 + C/(T-\theta)$, where χ_0 is the temperature independent susceptibility including Van-Vleck paramagnetism and core diamagnetism. The fitted Weiss temperature is $\theta = -59$ K. The value of $|\theta|$ is slightly larger than T_N, and the negative sign indicates the dominant AFM interaction in CMFMO. According to the Curie constant we obtained during the fitting ($C = 19.22$ emu·K/mol), the effective moment is calculated to be $\mu_{eff} = 12.4\ \mu_B$/fu. This value is comparable with the spin-only theoretical one (13.86 μ_B/fu) for CMFMO with the charge format of $CaMn^{3+}{}_3(Fe^{3+}{}_3Mn^{4+})O_{12}$, agreeing well with the XAS results.

The isothermal magnetization was measured at selected temperatures as shown in Fig. 3c. At the temperature well above T_N, e.g. at 200 K, the linear magnetization behavior is consistent with the paramagnetism. Near T_N such as at 50 and 30 K, however, the magnetization deviates from the linear dependence on field, but there is no visible magnetic hysteresis. It means that some short-range FM-like

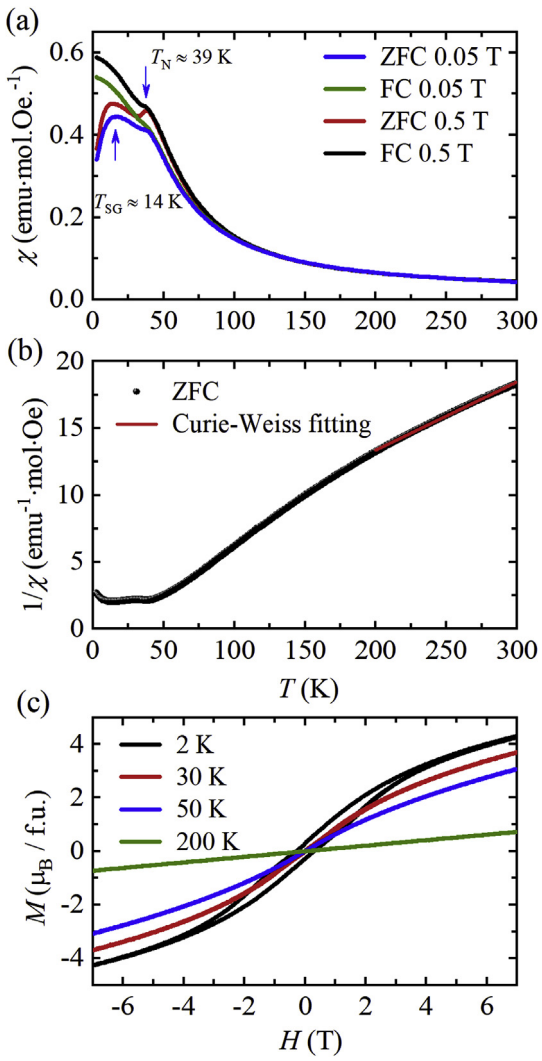

Fig. 3. (a) Temperature dependence of magnetic susceptibility measured at 0.05 and 0.5 T. (b) The inverse susceptibility and the Curie-Weiss fitting above 200 K. (c) Isothermal magnetization measured at selected temperatures.

correlations may form at lower temperatures. Below the spin glass transition temperature (e.g. at 2 K), one can find remarkable hysteresis as well as unsaturated magnetization behavior with field up to 7 T, implying the presence of competing FM and AFM interactions. Note that during the structure refinement, a small amount of α-Fe_2O_3 impurity phase (~ 5 wt%) is observed (see Fig. 1b). However, the impurity effect on the intrinsic magnetism of CMFMO is negligible since one cannot discern the spin transition of α-Fe_2O_3 occurring near 260 K [45] and that this critical temperature is far away from the T_N and T_{SG}, as represented in Fig. 3a.

In order to deeply investigate the magnetism of CMFMO, the ac magnetization as a function of temperature was measured at different frequencies from 133 Hz to 6333 Hz. As shown in Fig. 4, the ac susceptibility shows a frequency independent anomaly at T_N, confirming the long-range AFM phase transition occurring at this temperature. On further cooling to around 15 K, a broadening peak can be found. Moreover, with increasing frequency, the peak position shifts towards higher temperatures along with a reduction in the intensity, indicating the occurrence of a spin glass transition. Moreover, the characteristic frequency dependence of freezing temperature T_f in CMFMO can be well described by the conventional critical slowing down behavior with the model $\tau_f = \tau_0(T_f/T_g - 1)^{-z\nu}$ [46]. Here $z\nu$ is the dynamical exponent, $\tau_f = 1/f$ is the relaxation time related with the measurement frequency f,

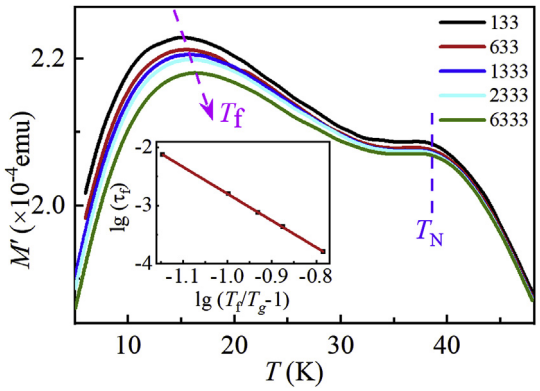

Fig. 4. Temperature dependent ac magnetization. The inset shows the plot of $\lg(\tau_f)$ vs $\lg(T_f/T_g\text{-}1)^{-z\nu}$ and the fitting result.

τ_0 is the intrinsic relaxation time of a single spin flip, and $T_g \approx 15.5$ K is the freezing temperature at $f = 0$ by extrapolating the T_f versus f. As shown in the inset of Fig. 4, we obtained the fitting parameters using this function, yielding $\tau_0 = 3.77(3) \times 10^{-8}$ s and $z\nu = 4.63(3)$. The expected value of $z\nu$ for a spin glass system usually varies from 4 to 12 [47]. For the cluster spin glass and canonical spin glass, the value of τ_0 ranges from 10^{-7} to 10^{-10} s and 10^{-12} to 10^{-13} s, respectively [48,49]. On the basis of the value of $z\nu$, we conclude that cluster spin glass should form in CMFMO.

We now discuss the origins for the two magnetic transitions occurring in CMFMO. As mentioned above, the A-site ordered $AMn_3B_4O_{12}$ perovskites usually exhibit two independent magnetic phase transitions originating from the A′-site Mn^{3+} and the B-site magnetic ions, respectively. Moreover, the A′-site Mn^{3+} spins often antiferromagnetically order at a critical temperature about 40–50 K, as shown in $YMn_3Al_4O_{12}$ [43] and La/$BiMn_3Cr_4O_{12}$ [16,17] etc. Taking into account the disorder Mn^{4+}/Fe^{3+} distribution as well as the similar T_N of CMFMO with those observed in other isostructural compounds [24,33,50], the long-range AFM ordering observed at 39 K is attributed to the A′-site Mn^{3+} ions, while the cluster spin glass arises from the competing FM and AFM interactions due to the random distribution of Fe^{3+} and Mn^{4+} at the B site in CMFMO. According to the Goodenough-Kanamori-Anderson rules [51–53], the $Fe^{3+}(3\,d^5)$-O-$Mn^{4+}(3\,d^3)$ superexchange pathways in a perovskite structure can generate FM interactions, whereas both Fe^{3+}-O-Fe^{3+} and Mn^{4+}-O-Mn^{4+} superexchange pathways give rise to AFM correlations. Therefore, the randomly distributed Fe^{3+} and Mn^{4+} would cause competing FM and AFM interactions, which are responsible for the cluster spin glass behavior.

Resistivity and specific heat were measured to characterize the transport properties of CMFMO. Fig. 5a presents temperature dependent electrical resistivity $\rho(T)$ measured at zero field. With decreasing temperature, the resistivity increases rapidly from 324 Ω cm at 300 K to 323 kΩ cm at 155 K, indicating the insulating behavior. In CMFMO, the A′-site MnO_4 units are spatially isolated from each other, the corner-sharing Mn/FeO_6 octahedra at the B site will dominate the electrical transport. Between 155 and 300 K, the resistivity data of CMFMO well follow the 3D Mott variable-range hopping model with the formula $\rho(T) = \rho_0 \exp(T_0/T)^{1/4}$, in accordance with the insulating feature due to the strong electron correlation effects of Fe^{3+} and Mn^{4+} [54].

Fig. 5b shows the temperature dependence of specific heat. Corresponding to the long-range AFM phase transition, the specific heat experiences a kink at T_N. However, near T_f, one cannot find any anomaly, as expected from the spin glass behavior. At lower temperatures (<12 K), the specific heat can be well fitted by the formula $C_p = \beta T^3 + \alpha T^{3/2}$ (see the inset of Fig. 5b) [55], yielding the coefficient $\beta = 7.2(4) \times 10^{-4}$ J/mol·K^4 and $\alpha = 8.9(1) \times 10^{-2}$ J/mol·$K^{5/2}$. The T^3 term represents phonon and AFM contributions, and the $T^{3/2}$ term results from the competing FM contribution, as reported in other spin glass systems [56,57]. The lack of T term is in agreement with the insulating feature of CMFMO at low temperature.

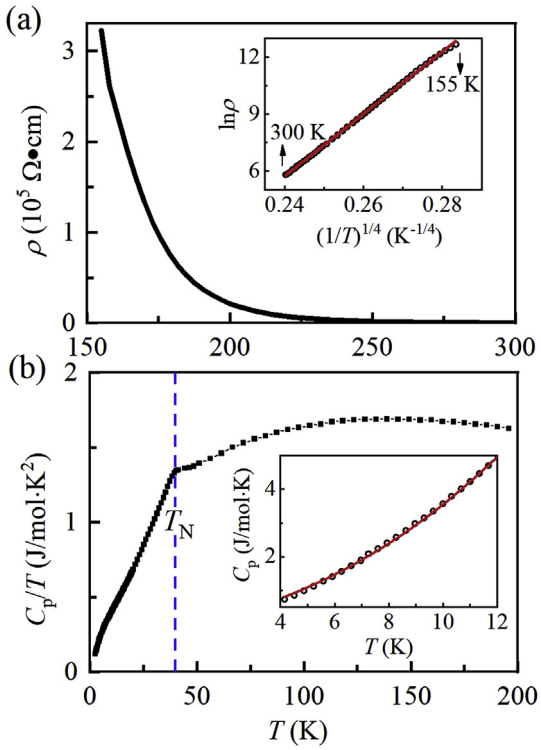

Fig. 5. (a) Temperature dependence of resistivity of $CaMn_3Fe_3MnO_{12}$. The inset shows the fitting result by the 3D variable-range hopping model between 155 and 300 K. (b) Specific heat as a function of temperature. The inset shows the low-temperature fitting result between 4 and 12 K using the formula $C_p = \beta T^3 + \alpha T^{3/2}$.

4. Conclusion

In summary, we are succeed in preparing a new oxide $CaMn_3Fe_3MnO_{12}$ at high pressure and high temperature. XRD and SAED show that this compound crystallizes in an A-site ordered perovskite structure with space group *Im*-3, indicating disorder distribution of Mn and Fe at the B site. On the basis of BVS calculations and XAS results, the charge states are determined to be $CaMn^{3+}{}_3(Fe^{3+}{}_3\,Mn^{4+})O_{12}$. A long-range AFM transition is observed at 39 K due to the spin ordering of A′-site Mn^{3+} ions. As the temperature further decreases to about 14 K, the compound shows a cluster spin glass transition due to the competing FM and AFM interactions generated by the randomly distributed Fe^{3+} and Mn^{4+} magnetic ions at the B site. The temperature dependent resistivity of CMFMO well follows the 3D Mott variable-range hopping mechanism, revealing the insulating behavior due to the strong electron correlation effects of Fe^{3+} and Mn^{4+}.

Acknowledgments

This work was supported by the National Key R&D Program of China (Grant No. 2018YFA0305700, 2018YFE0103200), the National Natural Science Foundation of China (Grant No. 51772324, 11574378), and the Chinese Academy of Sciences (Grant No. QYZDB–SSW–SLH013, GJHZ1773). We acknowledge the support from the Max Planck-POSTECH-Hsinchu Center for Complex Phase Materials.

References

[1] Y.W. Long, N. Hayashi, T. Saito, M. Azuma, S. Muranaka, Y. Shimakawa, Temperature-induced A-B intersite charge transfer in an A-site-ordered $LaCu_3Fe_4O_{12}$ perovskite, Nature 458 (7234) (2009) 60–63.

[2] Y. Shimakawa, Crystal and magnetic structures of $CaCu_3Fe_4O_{12}$ and $LaCu_3Fe_4O_{12}$: distinct charge transitions of unusual high valence Fe, J. Phys. D Appl. Phys. 48 (50) (2015), 504006.

[3] I. Yamada, K. Shiro, H. Etani, S. Marukawa, N. Hayashi, M. Mizumaki, Y. Kusano, S. Ueda, H. Abe, T. Irifune, Valence transitions in negative thermal expansion material $SrCu_3Fe_4O_{12}$, Inorg. Chem. 53 (19) (2014) 10563–10569.

[4] Y.W. Long, T. Saito, T. Tohyama, K. Oka, M. Azuma, Y. Shimakawa, Intermetallic charge transfer in A-site-ordered double perovskite $BiCu_3Fe_4O_{12}$, Inorg. Chem. 48 (17) (2009) 8489–8492.

[5] Y.W. Long, Y. Shimakawa, Intermetallic charge transfer between A-site Cu and B-site Fe in A-site-ordered double perovskites, New J. Phys. 12 (2010), 063029.

[6] K. Takata, I. Yamada, M. Azuma, M. Takano, Y. Shimakawa, Magnetoresistance and electronic structure of the half-metallic ferrimagnet $BiCu_3Mn_4O_{12}$, Phys. Rev. B 76 (2) (2007), 024429.

[7] X. Wang, M. Liu, X.D. Shen, Z.H. Liu, Z.W. Hu, K. Chen, P. Ohresser, L. Nataf, F. Baudelet, H.-J. Lin, C.-T. Chen, Y.-L. Soo, Y.-f. Yang, C.Q. Jin, Y.W. Long, High-temperature ferrimagnetic half metallicity with wide spin-up energy gap in $NaCu_3Fe_2Os_2O_{12}$, Inorg. Chem. 58 (1) (2019) 320–326.

[8] M. Etter, M. Isobe, H. Sakurai, A. Yaresko, R.E. Dinnebier, H. Takagi, Charge disproportionation of mixed-valent Cr triggered by Bi lone-pair effect in the A-site-ordered perovskite $BiCu_3Cr_4O_{12}$, Phys. Rev. B 97 (19) (2018) 195111.

[9] Y. Shimakawa, M. Takano, Charge disproportionation and charge transfer in A-site ordered perovskites containing iron, Z. Anorg. Allg. Chem. 635 (12) (2009) 1882–1889.

[10] I. Yamada, K. Takata, N. Hayashi, S. Shinohara, M. Azuma, S. Mori, S. Muranaka, Y. Shimakawa, M. Takano, A perovskite containing quadrivalent iron as a charge-disproportionated ferrimagnet, Angew. Chem. Int. Ed. 47 (37) (2008) 7032–7035.

[11] J.A. Alonso, J. Sanchez-Benitez, A. De Andres, M.J. Martinez-Lope, M.T. Casais, J.L. Martinez, Enhanced magnetoresistance in the complex perovskite $LaCu_3Mn_4O_{12}$, Appl. Phys. Lett. 83 (13) (2003) 2623–2625.

[12] X.-J. Liu, H.-P. Xiang, P. Cai, X.-F. Hao, Z.-J. Wu, J. Meng, A first-principles study of the different magnetoresistance mechanisms in $CaCu_3Mn_4O_{12}$ and $LaCu_3Mn_4O_{12}$, J. Mater. Chem. 16 (43) (2006) 4243–4248.

[13] Z. Zeng, M. Greenblatt, M.A. Subramanian, M. Croft, Large low-field magnetoresistance in perovskite-type $CaCu_3Mn_4O_{12}$ without double exchange, Phys. Rev. Lett. 82 (15) (1999) 3164–3167.

[14] C.C. Homes, T. Vogt, S.M. Shapiro, S. Wakimoto, A.P. Ramirez, Optical response of high-dielectric-constant perovskite-related oxide, Science 293 (5530) (2001) 673–676.

[15] T.B. Adams, D.C. Sinclair, A.R. West, Giant barrier layer capacitance effects in $CaCu_3Ti_4O_{12}$ ceramics, Adv. Mater. 14 (18) (2002) 1321–1323.

[16] X. Wang, Y.S. Chai, L. Zhou, H.B. Cao, C.D. Cruz, J.Y. Yang, J.H. Dai, Y.Y. Yin, Z. Yuan, S.J. Zhang, R.Z. Yu, M. Azuma, Y. Shimakawa, H.M. Zhang, S. Dong, Y. Sun, C.Q. Jin, Y.W. Long, Observation of magnetoelectric multiferroicity in a cubic perovskite system: $LaMn_3Cr_4O_{12}$, Phys. Rev. Lett. 115 (8) (2015) 087601.

[17] L. Zhou, J.H. Dai, Y.S. Chai, H.M. Zhang, S. Dong, H.B. Cao, S. Calder, Y.Y. Yin, X. Wang, X.D. Shen, Z.H. Liu, T. Saito, Y. Shimakawa, H. Hojo, Y. Ikuhara, M. Azuma, Z.W. Hu, Y. Sun, C.Q. Jin, Y.W. Long, Realization of large electric polarization and strong magnetoelectric coupling in $BiMn_3Cr_4O_{12}$, Adv. Mater. 29 (44) (2017), 1703435.

[18] I. Yamada, K. Tsuchida, K. Ohgushi, N. Hayashi, J. Kim, N. Tsuji, R. Takahashi, M. Matsushita, N. Nishiyama, T. Inoue, T. Irifune, K. Kato, M. Takata, M. Takano, Giant negative thermal expansion in the iron perovskite $SrCu_3Fe_4O_{12}$, Angew. Chem. Int. Ed. 50 (29) (2011) 6579–6582.

[19] M.W. Lufaso, P.M. Woodward, Jahn-Teller distortions, cation ordering and octahedral tilting in perovskites, Acta Crystallogr. B: Struct. Sci. Cryst. Eng. Mater 60 (2004) 10–20.

[20] B. Bochu, J.C. Joubert, A. Collomb, B. Ferrand, D. Samaras, Ferromagnetic oxides $Ln^{3+}Cu_3\ Mn_4O_{12}$ (Ln = La to Lu and Y), J. Magn. Magn. Mater. 15 (8) (1980) 1319–1321.

[21] J. Sanchez-Benitez, J. Antonio Alonso, M. Jesus Martinez-Lope, A. de Andres, M. Teresa Fernandez-Diaz, Enhancement of the Curie temperature along the perovskite series $RCu_3Mn_4O_{12}$ driven by chemical pressure of R^{3+} cations (R = Rare Earths), Inorg. Chem. 49 (12) (2010) 5679–5685.

[22] T. Saito, W.-t. Chen, M. Mizumaki, J.P. Attfield, Y. Shimakawa, Magnetic coupling between A' and B sites in the A-site-ordered perovskite $BiCu_3Mn_4O_{12}$, Phys. Rev. B 82 (2) (2010), 024426.

[23] G.Q. Zhang, S. Dong, Z.B. Yan, Y.Y. Guo, Q.F. Zhang, S. Yunoki, E. Dagotto, J.M. Liu, Multiferroic properties of $CaMn_7O_{12}$, Phys. Rev. B 84 (17) (2011), 174413.

[24] Y.W. Long, T. Saito, M. Mizumaki, A. Agui, Y. Shimakawa, Various valence states of square-coordinated Mn in A-site-ordered perovskites, J. Am. Chem. Soc. 131 (44) (2009) 16244–16247.

[25] S.H. Lv, H.P. Li, X.J. Liu, J. Meng, Mn-Cr intersite independent magnetic behavior and electronic structures of $LaMn_3Cr_4O_{12}$: study from first-principles, J. Appl. Phys. 110 (2) (2011), 023711.

[26] X.Z. Lu, M.H. Whangbo, S. Dong, X.G. Gong, H.J. Xiang, Giant ferroelectric polarization of $CaMn_7O_{12}$ induced by a combined effect of Dzyaloshinskii-Moriya interaction and exchange striction, Phys. Rev. Lett. 108 (18) (2012), 187204.

[27] J.T. Zhang, X.M. Lu, J. Zhou, H. Sun, F.Z. Huang, J.S. Zhu, Magnetic properties and origins of ferroelectric polarization in multiferroic $CaMn_7O_{12}$, Phys. Rev. B 87 (7) (2013), 075127.

[28] R. Przenioslo, I. Sosnowska, E. Suard, A. Hewat, A.N. Fitch, Phase coexistence in the charge ordering transition in $CaMn_7O_{12}$, J. Phys. Condens. Matter 14 (23) (2002) 5747–5753.

[29] B. Bochu, J.L. Buevoz, J. Chenavas, A. Collomb, J.C. Joubert, M. Marezio, Bond lengths in $CaMn_3(Mn_4)O_{12}$: a new Jahn-Teller distortion of Mn^{3+} octahedra, Solid State Commun. 36 (2) (1980) 133–138.

[30] S.M. Souliou, Y. Li, X. Du, M. Le Tacon, A. Bosak, Soft-phonon-driven orbital order in $CaMn_7O_{12}$, Phys. Rev. B 94 (18) (2016), 184309.

[31] R. Przenioslo, I. Sosnowska, E. Suard, A. Hewat, A.N. Fitch, Charge ordering and anisotropic thermal expansion of the manganese perovskite $CaMn_7O_{12}$, Physica B 344 (1–4) (2004) 358–367.

[32] R.D. Johnson, L.C. Chapon, D.D. Khalyavin, P. Manuel, P.G. Radaelli, C. Martin, Giant improper ferroelectricity in the ferroaxial magnet $CaMn_7O_{12}$, Phys. Rev. Lett. 108 (6) (2012), 067201.

[33] R. Przenioslo, I. Sosnowska, D. Hohlwein, T. Hauss, I.O. Troyanchuk, Magnetic ordering in the manganese perovskite $CaMn_7O_{12}$, Solid State Commun. 111 (12) (1999) 687–692.

[34] M.M. Seikh, V. Caignaert, O.I. Lebedev, B. Raveau, Cubic structure and canted antiferromagnetism of $CaMn_7O_{12}$ doped with trivalent cations (Fe, Al, Cr), Solid State Commun. 180 (2014) 52–55.

[35] R.D. Shannon, Revised effective Ionic-Radii and systematic studies of interatomic distances in Halides and Chalcogenides, Acta Crystallogr. A 32 (1976) 751–767.

[36] Z. Kesic, I. Lukic, M. Zdujic, C. Jovalekic, V. Veljkovic, D. Skala, Assessment of $CaTiO_3$, $CaMnO_3$, $CaZrO_3$ and $Ca_2Fe_2O_5$ perovskites as heterogeneous base catalysts for biodiesel synthesis, Fuel Process, Technol. 143 (2016) 162–168.

[37] H.M. Rietveld, A Profile refinement method for nuclear and magnetic structures, J. Appl. Crystallogr. 2 (1969) 65–71.

[38] A.C. Larson, R.B. Von Dreele, General Structure Analysis System (GSAS); Report No. LAUR 86-748, Los Alamos National Laboratory, Los Alamos, NM, 1994.

[39] S.H. Byeon, S.S. Lee, J.B. Parise, P.M. Woodward, N.H. Hur, High-pressure synthesis of metallic perovskite ruthenate $CaCu_3Ga_2Ru_2O_{12}$, Chem. Mater. 16 (19) (2004) 3697–3701.

[40] S.H. Byeon, S.S. Lee, J.B. Parise, P.M. Woodward, N.H. Hur, New ferrimagnetic oxide $CaCu_3Cr_2Sb_2O_{12}$: high-pressure synthesis, structure, and magnetic properties, Chem. Mater. 17 (13) (2005) 3552–3557.

[41] N.E. Brese, M. Okeeffe, Bond-valence parameters for solids, Acta Crystallogr. Sect. B Struct. Sci. 47 (1991) 192–197.

[42] I.D. Brown, D. Altermatt, Bond-valence parameters obtained from a systematic analysis of the inorganic crystal-structure database, Acta Crystallogr. Sect. B Struct. Sci. 41 (1985) 244–247.

[43] T. Tohyama, T. Saito, M. Mizumaki, A. Agui, Y. Shimakawa, Antiferromagnetic interaction between A'-site Mn spins in A-site-ordered perovskite $YMn_3Al_4O_{12}$, Inorg. Chem. 49 (5) (2010) 2492–2495.

[44] T. Burnus, Z. Hu, H.H. Hsieh, V.L.J. Joly, P.A. Joy, M.W. Haverkort, H. Wu, A. Tanaka, H.J. Lin, C.T. Chen, L.H. Tjeng, Local electronic structure and magnetic properties of $LaMn_{0.5}Co_{0.5}O_3$ studied by x-ray absorption and magnetic circular dichroism spectroscopy, Phys. Rev. B 77 (12) (2008), 125124.

[45] N. Pattanayak, A. Bhattacharyya, S. Chakravarty, A. Bajpai, Weak ferromagnetism and time-stable remanence in hematite: effect of shape, size and morphology, J. Phys. Condens. Matter 31 (36) (2019), 365802.

[46] K. Binder, A.P. Young, Spin glasses: experimental facts, theoretical concepts, and open questions, Rev. Mod. Phys. 58 (4) (1986) 801–976.

[47] S. Pakhira, C. Mazumdar, R. Ranganathan, S. Giri, M. Avdeev, Large magnetic cooling power involving frustrated antiferromagnetic spin-glass state in R_2NiSi_3 (R = Gd, Er), Phys. Rev. B 94 (10) (2016), 104414.

[48] J. Lago, S.J. Blundell, A. Eguia, M. Jansen, T. Rojo, Three-dimensional Heisenberg spin-glass behavior in $SrFe_{0.90}Co_{0.10}O_{3.0}$, Phys. Rev. B 86 (6) (2012), 064412.

[49] A. Malinowski, V.L. Bezusyy, R. Minikayev, P. Dziawa, Y. Syryanyy, M. Sawicki, Spin-glass behavior in Ni-doped $La_{1.85}Sr_{0.15}CuO_4$, Phys. Rev. B 84 (2) (2011), 024409.

[50] Y.-Y. Yin, M. Liu, J.-H. Dai, X. Wang, L. Zhou, H.B. Cao, C. dela Cruz, C.-T. Chen, Y.J. Xu, X. Shen, R.C. Yu, J. Antonio Alonso, A. Munoz, Y.-F. Yang, C.Q. Jin, Z.W. Hu, Y.W. Long, $LaMn_3Ni_2Mn_2O_{12}$: an A- and B-site ordered quadruple perovskite with A-site tuning orthogonal spin ordering, Chem. Mater. 28 (24) (2016) 8988–8996.

[51] J.B. Goodenough, Theory of the role of covalence in the perovskite-type manganites [LA, M(II)] MnO_3, Phys. Rev. 100 (2) (1955) 564–573.

[52] J. Kanamori, Superexchange interaction and symmetry properties of electron orbitals, J. Phys. Chem. Solids 10 (2–3) (1959) 87–98.

[53] P.W. Anderson, Antiferromagnetism - theory of superexchange interaction, Phys. Rev. 79 (2) (1950) 350–356.

[54] P. Kayser, M.J. Martinez-Lope, J.A. Alonso, J. Sanchez-Benitez, M.T. Fernandez, High-pressure synthesis and characterization of $BiCu_3(Mn_{4-x}Fe_x)O_{12}$ (x=0, 1.0, 2.0) complex perovskites, J. Solid State Chem. 204 (2013) 78–85.

[55] V.K. Anand, D.T. Adroja, A.D. Hillier, Ferromagnetic cluster spin-glass behavior in $PrRhSn_3$, Phys. Rev. B 85 (1) (2012), 014418.

[56] J.M.D. Coey, S. Vonmolnar, R.J. Gambino, Magnetic heat capacity of an amorphous Gd-Al alloy, Solid State Commun. 24 (2) (1977) 167–170.

[57] J.O. Thomson, J.R. Thompson, Low-temperature excitations in spin glasses: evidence for a $T^{3/2}$ behavior, J. Phys. F Met. Phys. 11 (1) (1981) 247–260.